ACS APPLIED MATERIALS & INTERFACES

Research Article

www.acsami.org

Numerical Analysis of Electron Emission Site Distribution of Carbon Nanofibers for Field Emission Properties

Norihiro Shimoi*[,†] and Shun-ichiro Tanaka[‡]

[†]Graduate School of Environmental Studies, Tohoku University, 6-6-20 Aoba, Aramaki, Aoba-ku, Sendai 980-8579, Japan

[‡]Institute of Multidisciplinary Research for Advanced Materials, Tohoku University, 2-1-1 Katahira, Aoba-ku, Sendai 980-8577, Japan

ABSTRACT: To obtain optimal field emission (FE) properties, it is important to evaluate FE parameters including the electron emission site α and the field enhancement factor β. However, it is difficult to evaluate α quantitatively because the emitting electrons cannot be observed directly. The authors have aimed to analyze this site using an original architecture with a computation system tool based on the surface charge method, and a three-dimensional model has been employed to calculate FE properties with high accuracy. In this study, to analyze α for determining FE properties, each carbon nanofiber (CNF) model separated by Cr islands which include the minimum area for calculating electric fields by the surface charge method was constructed on the surface of a Ni catalyst. The FE current was simulated with a Fowler–Nordheim formula using the calculated electric fields, followed by a simulation performed using all CNFs on a field emitter cathode. The electron emission site α was determined by comparing the simulation and experimental results of the FE current. It was found that α depends on the morphology of the CNF bundles, and a close quantitative correspondence between the experimental and the computation results of FE properties was obtained. In summary, a method of analyzing FE properties was established using an original architecture, making it possible to predict FE properties with a computational tool based on the surface charge method.

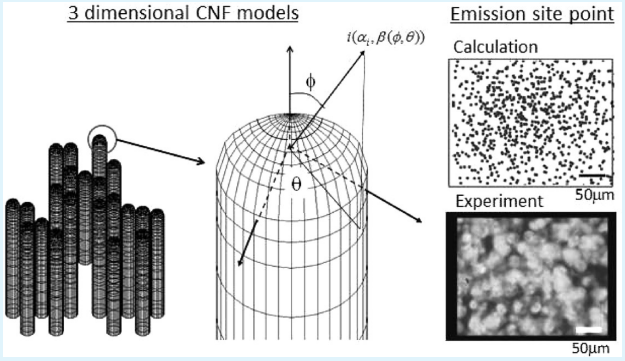

KEYWORDS: *field emission, carbon nanofiber, electron emission site, surface charge method*

I. INTRODUCTION

Since field emission (FE) using a carbon nanotube (CNT) was first reported in a landmark paper by Rinzler et al.,[1] CNTs and carbon nanofibers (CNFs) have attracted considerable attention as FE sources. To assemble the cathode of a FE device with high-efficiency brightness, it is important for such a device to emit electrons with high efficiency and low drive voltage. Many studies seeking to control the shape and density of CNTs or CNFs have been carried out to achieve adequate FE properties. Thus, evaluation of FE parameters including the field enhancement factor β and the electron emission site α is important for the control of FE characteristics. Many researchers have verified the field enhancement factor β by simply evaluating the synthesis morphology or shape of the CNF emitters. To obtain a favorable β, it is effective to decrease rod diameter and sharpen the actual top of the CNF. However, another FE parameter, the electron emission site α, has hardly been discussed because it is impossible to observe areas of electron emission directly except in a projection image of electrons emitting from a few CNT/CNFs.[2,3] Generally, an electron emission site is obtained using an observed current–voltage (I–V) characteristic curve followed by translation to a plot on the basis of the Fowler–Nordheim formula.[4] Some reports have discussed, the correlation between the emission site area results obtained from I–V characteristics and the synthesis morphology of CNT/CNFs obtained experimentally.[5−11] They note that control of the morphology including synthesis bundle size, length, and diameter of CNT/CNFs is effective for the optimization of the emission site from a statistical point of view.[12−16] A model of FE site density obtained from experimental results was proposed empirically by Liu et al.[17,18] However, the construction of a model for verifying emission sites and simulating the design of emission sites has yet to be realized.

This study aimed to analyze the mechanism of the electron emission site α with an original simulation model, constructing and employing a computation system for simulating an electrical or magnetic field with a three-dimensional model based on the surface charge method.[19] This simulation program is available for constructing complex and optional shapes and for calculating minute models on a nanometer scale. To evaluate FE parameters with this simulation tool, a CNF model was designed on the basis of actual CNFs by controlling synthesis morphology. Figure 1 shows the synthesis results in ref 16. Each CNF on the Ni–Cr alloy catalyst shows favorable growth alignment and positive shape including uniform

Received: October 15, 2012
Accepted: December 28, 2012
Published: December 28, 2012

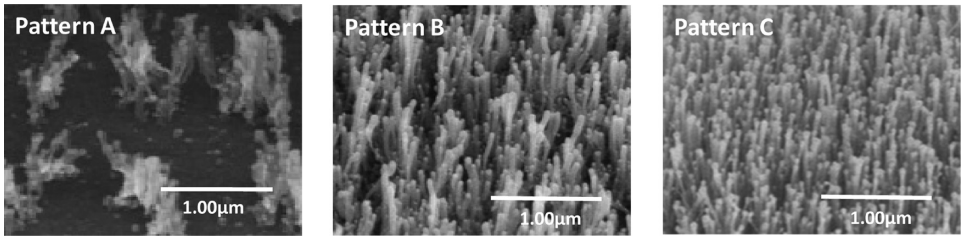

Figure 1. Morphology of synthesized CNFs depending on Ni contents in the Ni−Cr alloy catalyst in ref 16.

diameter and uniform rod height form. CNFs were synthesized on a nickel catalyst separated by chromium grains grown by co-sputtering Ni and Cr.

The FE characteristics of electrons emitted from CNF bundles to obtain the emission site area were evaluated on the basis of current−voltage (I−V) curves obtained using an apparatus with at least a cathode and an anode maintaining at 100 μm. I−V curves are measured currents flowing as a result of applying bias voltage between opposite electrodes at each 1 mm^2. The experimental electron emission site is obtained from a slope and intercept of a curve transforming I−V curve results.[16]

II. SIMULATION PROCEDURES AND ARCHITECTURE FOR EMISSION SITE AREAS

II-a. Modeling Morphology of Specimens. Simulation models based on the design rule in Figure 2[16] confirmed in this

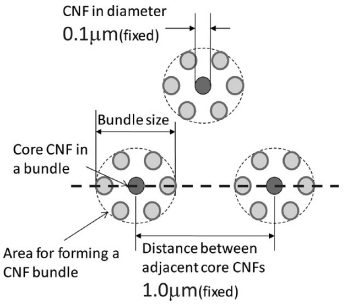

Figure 2. Design rule of CNF array patterning.

study that the electron emission site α, which is essential for the analysis of FE properties, could be analyzed using a systematic architecture. This method is therefore available for the analysis of electron emission sites for FE emitters with any material or shape. Further, the morphology and distribution of FE emitters can be optimized by computation and appropriately designed to obtain excellent FE properties. Each CNF model in diameter fixed at 0.1 μm from a measurement average of actual CNF is aligned vertically in this simulation. Millions of modeled CNFs are arrayed on a cathode plane in a 1 mm^2 region based on experimental conditions of FE measurements. Figure 2 shows on basic parts of CNFs arraying model. CNF array models in Figure.2 with a core CNF fixed at the position and CNFs arranged like a hexagonal pack around a core CNF. The distance between adjacent core CNFs, which is decided from an averaged distance of CNFs of Pattern A in Figure.1, is fixed at 1.0 μm, so CNF bundle size is controlled by changing the number of CNFs surrounding a core. Furthermore, the space distance between adjacent CNFs is controlled by a simulation program to prevent from a model failure of hexagonal packed arrangement of CNFs.

Figure 3 shows the morphology of the CNFs grown using CH_4/H_2/He gases on Ni grains in a Ni−Cr alloy from Figure 1.

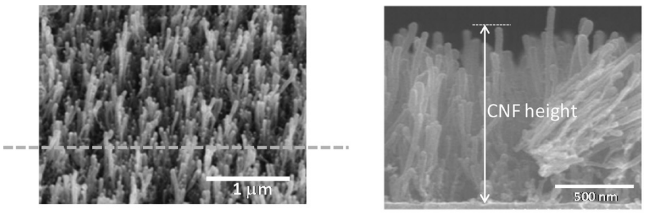

(a) Morphology of Pattern B (b) Cross-sectional view of CNFs

Figure 3. SEM images for measuring CNF height in Pattern B in Figure 1.

Well-controlled growth of CNFs is demonstrated on the Ni−Cr alloy catalyst in Figure 3a, and the distance between CNF bundles depended on the nickel content of the alloy. In this case, the nickel content of the Ni−Cr catalyst shown in Figure 3a was 57 wt %.[16] Figure 3b shows cross-sectional views of the CNFs near the dotted line in Figure 3a. Although these results indicate that the nickel on the Ni−Cr alloy catalyst layer assisted CNF growth in a vertical direction and determined the shape of CNFs, the distribution of CNF height is a little uneven, as seen in Figure 3b.

This height distribution is graphed in Figure 4. CNF height exhibited an approximately normal distribution; the average CNF height was near 1.0 μm, and the standard deviation was near 0.13 μm. These results indicate that uniform CNFs are synthesized at a temperature lower than the glass transition

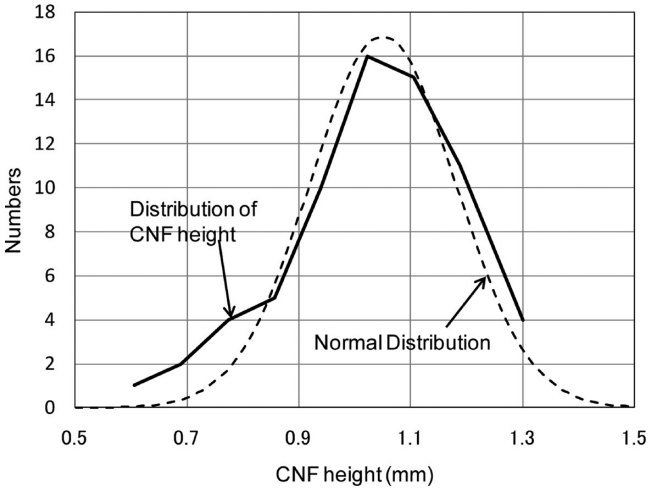

Figure 4. Normalized heights of CNFs on randomly grown FE cathodes showing a uniform distribution of CNF height. In our model, the maximum CNF height is 1.3 μm, and the CNF simulation model was designed with this distribution.

dx.doi.org/10.1021/am302324w | ACS Appl. Mater. Interfaces 2013, 5, 768−773

temperature. Thus, in this study, a simulation model for evaluating FE characteristics was simply constructed with a model of small CNF bundles on an FE cathode whose morphology is close to that shown in Figure 3b. The height of each CNF for simulation was arrayed randomly by using random digits code of a computational language within a normal distribution from 0.6 to 1.5 μm of CNF height as shown in Figure 4. The height stride was 0.05 μm in this study. Figure 5 shows a part of a schematic model used to calculate for the analysis of FE characteristics based on the above modeling rule.

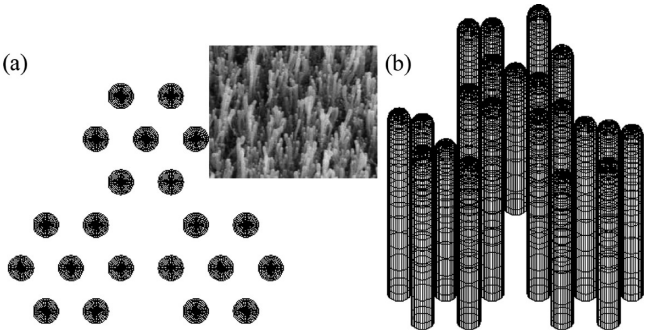

Figure 5. Schematic models used to calculate the electrical fields and equipotential lines. Panel (a) shows a top view of CNF bundle arrays with a uniform distance between CNF bundles. The inset in panel (a) shows a photograph of the original CNF distribution as an example whereas panel (b) shows a simple imitation of a computational model in which CNFs stand in three dimensions. One bundle consists of the simplified CNF meshed elements shown in panel (b) which enable the computation.

In this study, a computation program was employed with a calculation code based on the surface charge method which is one of the integral element methods. In this calculation method it is easy to construct 3-dimensional models optionally available for the calculation of electrical or magnetic distribution because it is unnecessary to make the mesh in space.[20] The source code and calculation module were originally written at the Sony Corporation, and the customization of the calculation module and the construction of the computation model were carried out at Tohoku University. In this study, the calculated model was composed of a diode structure with an anode for loading bias voltage and a cathode on which CNFs stand; the shape and arrangement of these CNFs were modeled systematically.

II-b. Simulation Architecture for Emission Site Areas. Figure 6 shows the model concept defining the emission site area α. The distribution of the electric field on a CNF was calculated using a unique simulation program, and the area on which electrons emit from the surface of a CNF was guided. The surface of a CNF was divided into several small areas as the electron emission sites. The sum of currents calculated on each area is equivalent to the current flowing from a CNF, and the total current on the cathode is defined as the sum of the current on each CNF. The electron emission site was determined when the above calculated current was equal to the experimental current–voltage characteristics. The equation of this concept is as follows:

$$I_j = \sum_j (N_j \times i_{\mathrm{dens}} \times \alpha_j) \tag{1}$$

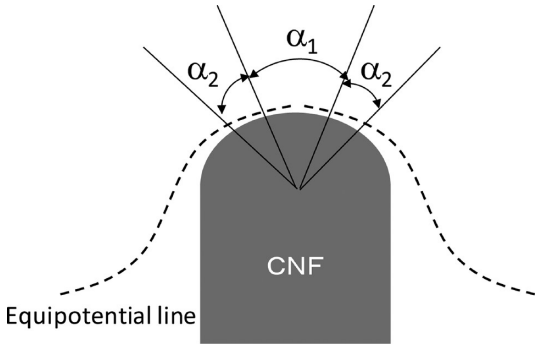

Figure 6. Model showing a determination of an electron emission site on a CNF. The site α_j (j = 1,2, ...) is partitioned by the strength of electric field numerically, with the total area of α_i defined as a FE electron emission site.

where α_j shows the units of the electron emission site on a CNF, i_{dens} is the calculated current density obtained from a unit, N_j is the number of CNFs emitting electrons, and I_j is the total current from the cathode.

Figure 7 shows the conceptual array of the computation models. Although each CNF is 100 nm in diameter, the height

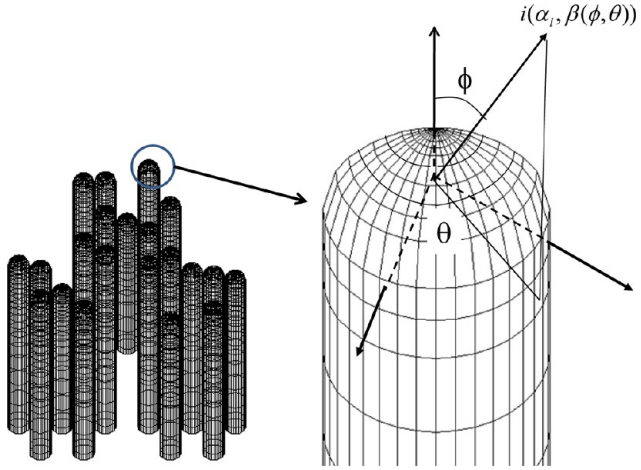

Figure 7. Simulation model of a CNF imitating the growth of CNFs in Figure 3a. A CNF model with a hemispheric cap that covers the top of a CNF simplified using a randomly distributed normal height. The surface of the CNF is divided for calculating elements by the surface charge method. The center of the hemisphere on the top of the CNF is defined as the origin of polar coordinates. The total current obtained from each element consisting of the FE current on a CNF and the total current from CNFs on the cathode corresponds to the experimental FE current.

of each CNF is randomly decided following the distribution shown in Figure 3b. A hemispherical cap covers the top of each CNF, and the surface of a CNF is divided for calculating elements by the surface charge method. It is possible to calculate fields on each element in this model and simulate an FE current. The current from a CNF (I_{CNF}) is calculated using a model based on Figure 7b:

$$I_{\mathrm{CNF}} = \iint i(\alpha_i, \beta(\phi, \theta))\, \mathrm{d}\phi\, \mathrm{d}\theta \tag{2}$$

where $i(\alpha_i,\beta(\phi,\theta))$ shows the current simulated from an element divided by the framework in Figure 7b, α_i is the electron emission site area from an element, and $\beta(\phi,\theta)$ is the

dx.doi.org/10.1021/am302324w | ACS Appl. Mater. Interfaces 2013, 5, 768–773

field enhancement factor on an element simulated from the CNF model in Figure 7b. This field enhancement factor is the ratio of the electric field between free spaces to the concentrated field on an element. The detailed scalar amount of the electric field is calculated to be 3 nm above the CNF model's surface. This distance is estimated from the thickness of the electron tunnel barrier when electrons cause Fowler–Nordheim tunneling.[21] The center of the hemisphere on the top of a CNF is defined as the origin of polar coordinates, with ϕ and θ being the polar and azimuth angles based on these coordinates. ϕ and θ were chosen at angles with the emission current at 1/100 of the maximum current $i(\alpha,\beta(\phi,\theta))$. The lower limit 1/100 was decided as a value when the total calculated current obtained from all modeled CNFs on a cathode was the same as a measured FE current experimentally. Figure 8 shows examples of the calculated results when either ϕ

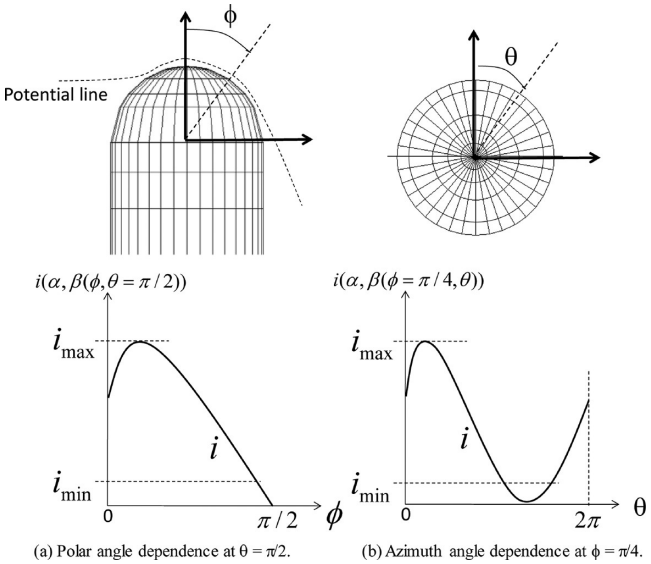

Figure 8. Examples of an electric field and current calculated at $\theta = \pi/6$ or $\phi = \pi/4$, defined as the polar and azimuth angles, respectively. i_{max} is the maximum current calculated on an element on a CNF; in contrast, i_{min} is defined as that on 1% of i_{max}.

or θ is fixed. The potential on a CNF differs depending on the position where CNFs stand on a bundle or a cathode and on the CNF height. For example, Figure 8a shows the calculation of the current i when the polar angle ϕ is fixed at $\pi/2$. Figure 8b shows the result when the azimuth angle θ is $\pi/4$. In this case, the maximum ϕ and θ are within $\pi/2$ and 2π. Total current from CNFs on the cathode in Figure 3a is expressed by the following equations:

$$I_{bundle} = \sum I_{CNF} \quad (3)$$

$$I(\text{Cathode}) = I_{bundle} \times N \quad (4)$$

$$\alpha_{exp} = \sum \alpha_i \quad (5)$$

where I(Cathode) is equal to the total current calculated from all the CNFs on the cathode in Figure 1. This value is related to experimental FE current, and the summary of the emission site area α_i in eq 2 is a required emission site area for satisfying eq 3. The area for measuring FE current is determined by the anode size of the measurement equipment for current–voltage characteristics. The calculated current per CNF bundle is defined as I_{bundle}, and the number of CNF bundles, N, is estimated from the cathode area for FE emission. The total current from a sample is expressed by eq 4. The α_j in eq 2 is an important function for estimating the emission site area when comparing the FE current in eq 4 with the measured current. The authors presumed that experimental electron emission site α_{exp} in eq 5 was equivalent to the sum of α_j when the calculated result is equal to the experimental result.

III. COMPARISON OF NUMERICALLY CALCULATED RESULTS WITH EXPERIMENTAL RESULTS

The emission site area α was defined as the total area of elements calculated using the FE current mentioned in II. For example, the calculated area is shown in gray in Figure 9,

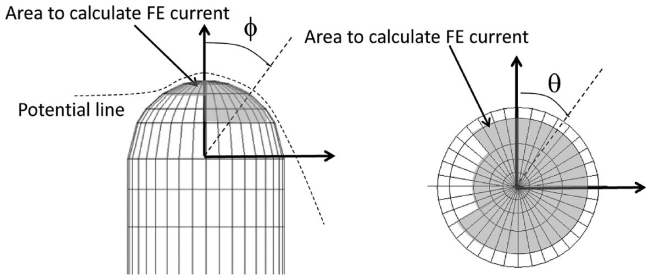

Figure 9. Emission site area determined as the total area for FE current calculation. The calculated area is shown in gray and is defined as the current threshold with 1% of the maximum current among all the elements of the CNF models.

defining that the current floating in an element is larger than the calculated current threshold, that is, i_{min}. In this case, the biased voltage on the anode in Figure 1 is typically 130 V. The calculation α obtained from the right side in eq 5 is determined when I(Cathode) in eq 4 is equal to the experimental FE current in ref 16.

Figure 10 shows the relationship between α and the size of the synthesized CNF bundle. α expresses both the experimental

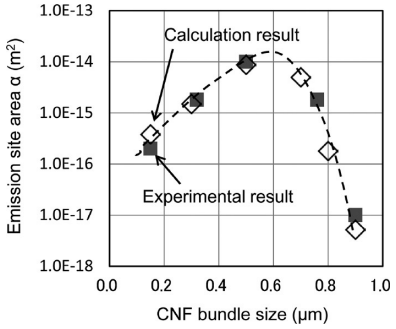

Figure 10. Calculated emission site area α depends on the CNF bundle size. There is a close relationship between experimental and calculated results.

results including morphology in Figure 1 and simulation results obtained from this study. An experimental CNF bundle size indicates an average size measured by SEM images. They are in good agreement quantitatively. This means that the architecture developed for theoretically obtaining the emission site area enables the analysis of FE characteristics, especially the experimental emission site area.

dx.doi.org/10.1021/am302324w | ACS Appl. Mater. Interfaces 2013, 5, 768–773

Evaluation of the α dependence obtained from experimental results was realized using simulation bundle models of the CNF surface morphology indicating clouds of bundle patterns. The authors proposed the algorithm of the fixed quantity analysis with a three-dimensional model of α, which has not yet been studied by numerical analysis. Figure 11 shows a comparison of

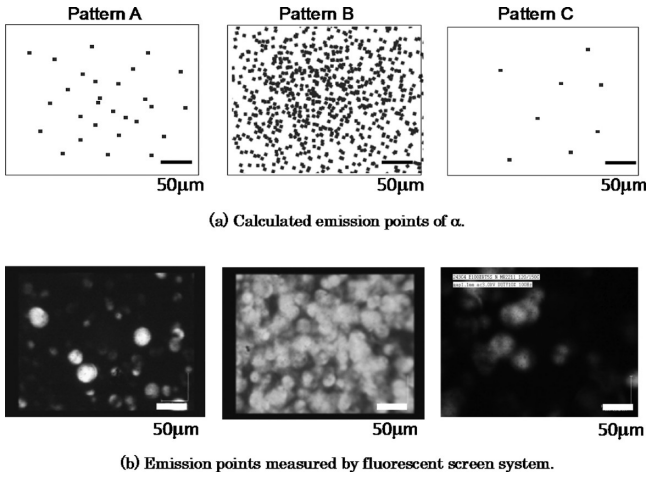

Figure 11. Comparison between the simulation and the measurement of FE emission points.

the site of CNFs between calculated results with FE from the simulation analysis method of α and the luminescence site obtained from the experiment with the diode measurement. The square points of (a) in Figure 11 indicate the CNFs with FE obtained from the calculation, and their distribution is similar to the distribution of the density of the luminous points obtained by the measurement in (b). Although the simulation models in (a) are constructed with a CNF density and height distribution based on the actual surface morphology of CNFs in (b), those patterns of simulation models differ considerably from the synthesis morphology in (b).

For Pattern A, the emission site on isolated CNFs is concentrated at several points. In Pattern B, the points of (a) mean the emission sites from higher CNFs located at the edge of the CNF bundles. Pattern C shows the morphology on which many short CNFs are arrayed over some protruding CNFs, and the concentrated electrical field strength on the top of longer CNFs for FE in Pattern C can be easily presumed to be weaker than the strength in Patterns A and B. Figure 12 shows an image indicating that the electrical field is concentrated over the CNFs in Pattern C.

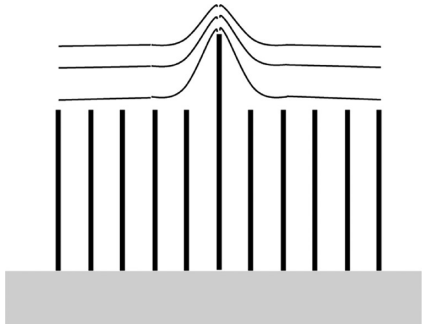

Figure 12. Equipotential line focused on a protruding CNF in Pattern C.

Accordingly, based on the height distribution of CNFs shown in Figure 4 for a normal distribution, the number ratio of CNFs used as the FE emitter is determined from the CNF height distribution. The height distribution of CNFs for FE is projected from the calculated model in Figure 11, and when the distribution of the height is applied to the distribution in Figure 4, CNFs existing near the top of the normal distribution are occupied by the emission site. Ultimately, the numbers of CNFs for FE are 3−5% of the total numbers of synthesized CNFs in the cases of Patterns A and C. Figure 13 shows the

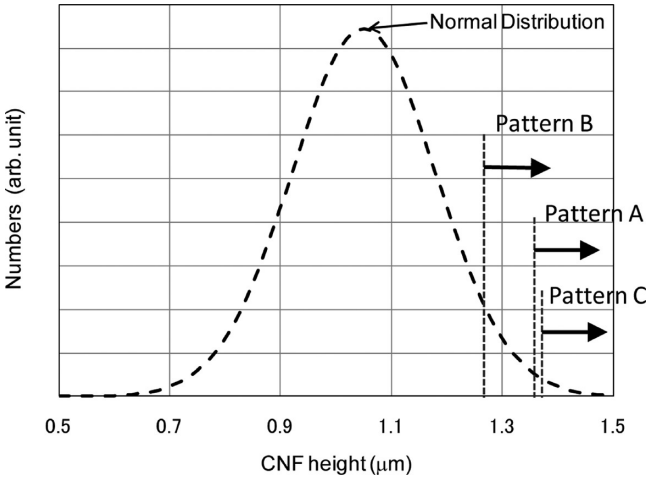

Figure 13. Calculated ratio of CNF numbers for FE from patterns A−C based on the emission site in Figure 11.

ratio of CNFs to emitted electrons in each pattern, compared by outlines in the CNF height distribution. The dotted line shows the ratio of the number of CNFs for calculating α to the total number of CNFs that gather in the simulation model, and the arrow signs on the right indicate the high distribution of CNFs used for the α calculation, these being higher than the CNFs on the dotted line.

The results above showed that 80% or more of the CNFs grown did not contribute to FE. To improve the FE property, the number of CNFs contributing to FE should perhaps be increased, implying that the difference in the ratio of CNFs contributing to the FE depends on the array patterning when the distributions of the CNF height are equal in all patterns.

IV. CONCLUSIONS

The electron emission site α was calculated using an original computation program based on the surface charge method with a three-dimensional model obtained from experimental CNF bundle morphologies. The model for the α analysis was constructed on the basis of CNF bundles uniformly standing on a patterned Ni catalyst. Each CNF had a straight alignment normal to the substrate, a rod of almost the same diameter, and the same shape covered with a hemispherical shape cap on its top. Synthesized morphology CNFs of random heights, which were normalized using the normal distribution in a CNF height histogram, were designed for the confirmation of the electron emission site α. With the above models, the top of a CNF was divided into several elements for calculating the FE current. This made it possible to analyze the emission site area α by a simulation employing an original architecture with a detailed calculation of the current from the top of a CNF. The electron emission site area α could be defined numerically and

quantitatively by the models on the basis of experimental results and expressed dependent on the array of the CNF bundles and the synthesized height of CNFs on the FE cathode. When using CNF bundles on a patterned catalyst with a controlled Ni−Cr content, α depends on CNF morphologies when using different synthesizing methods, particularly CNF bundle size and growth height. A CNF morphology with good FE characteristics resulting in a maximum-electron-emission site at a typical bias voltage is predicted to have a CNF bundle size close to 0.6 μm. It is possible to obtain FE properties using a computation model that includes FE parameters.

We intend to verify FE characteristics by determining synthesized size, FE emitter shape, and arraying distribution in a future study, since it is now possible to numerically obtain optimal FE properties by designing field emitter shape and array morphology.

AUTHOR INFORMATION

Corresponding Author

*Fax: +81-22-795-4584. E-mail: shimoi@mail.kankyo.tohoku.ac.jp.

Notes

The authors declare no competing financial interest.

ACKNOWLEDGMENTS

This work was partially supported by the Global COE Program "Materials Integration International Center of Education and Research, Tohoku University," MEXT, Japan.

REFERENCES

(1) Rinzler, A. G.; Hafner, J. H.; Nikolaev, P.; Lou, L.; Kim, S. G.; Tomanek, D.; Nordlander, P.; Colbert, D. T.; Smalley, R. E. *Science* **1995**, *269*, 1550−1553.
(2) Nemanic, V.; Zumer, M.; Zajec, B. *Ultramicroscopy* **2008**, *108*, 69−73.
(3) Kobayashi, S.; Saito, Y.; Mizusawa, T.; Shirai, K.; Latham, R. V.; Tajiri, K.; Yamanaka, Y. *Appl. Surf. Sci.* **1999**, *144−45*, 118−122.
(4) Spindt, C. A.; Brodie, I.; Humphrey, L.; Westerberg, E. R. *J. Appl. Phys.* **1976**, *47* (12), 5248−5263.
(5) Manohara, H. M.; Bronikowski, M. J.; Hoenk, M.; Hunt, B. D.; Siegel, P. H. *J. Vac. Sci. Technol.* **2005**, *B 23* (1), 157−161.
(6) Shang, N. G.; Papakonstantinou, P.; McLaughlin, J.; Chen, W. C.; Chen, L. C.; Chu, M.; Stamboulis, A. *J. Appl. Phys.* **2008**, *103*, 124308.
(7) Zhang, J. H.; Feng, T.; Yu, W. D.; Liu, X. H.; Wang, X.; Li, Q. *Diamond Relat. Mater.* **2004**, *13*, 54−59.
(8) Groning, O.; Clergereaux, R.; Nilsson, L. O.; Ruffieux, P.; Groning, P.; Schlapbach, L. *Chimia* **2002**, *56*, 553−561.
(9) Wang, Y. H.; Lin, J.; Huan, C. H. A. *Thin Solid Films* **2002**, *405*, 243−247.
(10) Shiffler, D.; Zhou, O.; Bower, C.; LaCour, A.; Golby, K. *IEEE Trans. Plasma Sci.* **2004**, *32*, 2152−2154.
(11) Wang, L. Y.; Wang, X. P.; Wang, L. J.; Zhang, L. *Chin. Phys. Lett.* **2008**, *25*, 4154−4157.
(12) Bronikowski, M. J.; Manohara, H. M.; Hunt, B. D. *J. Vac. Sci. Technol.* **2006**, *A 24* (4), 1318−1322.
(13) Zhang, H. Z.; Zhao, Q.; Yu, J.; Yu, D. P.; Chen, Y. *J. Phys. D: Appl. Phys.* **2007**, *40*, 144−147.
(14) Park, K. H.; Lee, S.; Kohb, K. H. *J. Appl. Phys.* **2006**, *99*, 034303.
(15) Frolov, V. D.; Karabutov, A. V.; Pimenov, S. M.; Konov, V. I. *Diamond Relat. Mater.* **2000**, *9*, 1196−1200.
(16) Shimoi, N.; Tanaka, S.-I. *Carbon* **2009**, *47*, 1258−1263.
(17) Liu, H.; Kato, S.; Saito, Y. *Nanotechnology* **2009**, *20*, 275206.
(18) Liu, H.; Kato, S.; Saito, Y. *Jpn. J. Appl. Phys.* **2009**, *48*, 015007.
(19) Shimoi, N.; Tanaka, S.-I. *Carbon* **2010**, *48*, 905−911.
(20) Murata, H.; Shimoyama, H.; Ohye, T. *Proc. SPIE* **2001**, *4510*, 156.
(21) Gomer, R. *Field emission and field ionization*; Harvard University Press.: Cambridge, MA, 1961; p 32.